Diagn Interv Radiol 2017; 23:227–232

INTERVENTIONAL RADIOLOGY

ORIGINAL ARTICLE

1.5 T augmented reality navigated interventional MRI: paravertebral sympathetic plexus injections

David R. Marker
Paweena U-Thainual
Tamas Ungi
Aaron J. Flammang
Gabor Fichtinger
Iulian I. Iordachita
John A. Carrino
Jan Fritz

PURPOSE
The high contrast resolution and absent ionizing radiation of interventional magnetic resonance imaging (MRI) can be advantageous for paravertebral sympathetic nerve plexus injections. We assessed the feasibility and technical performance of MRI-guided paravertebral sympathetic injections utilizing augmented reality navigation and 1.5 T MRI scanner.

METHODS
A total of 23 bilateral injections of the thoracic (8/23, 35%), lumbar (8/23, 35%), and hypogastric (7/23, 30%) paravertebral sympathetic plexus were prospectively planned in twelve human cadavers using a 1.5 Tesla (T) MRI scanner and augmented reality navigation system. MRI-conditional needles were used. Gadolinium-DTPA-enhanced saline was injected. Outcome variables included the number of control magnetic resonance images, target error of the needle tip, punctures of critical nontarget structures, distribution of the injected fluid, and procedure length.

RESULTS
Augmented-reality navigated MRI guidance at 1.5 T provided detailed anatomical visualization for successful targeting of the paravertebral space, needle placement, and perineural paravertebral injections in 46 of 46 targets (100%). A mean of 2 images (range, 1–5 images) were required to control needle placement. Changes of the needle trajectory occurred in 9 of 46 targets (20%) and changes of needle advancement occurred in 6 of 46 targets (13%), which were statistically not related to spinal regions ($P = 0.728$ and $P = 0.86$, respectively) and cadaver sizes ($P = 0.893$ and $P = 0.859$, respectively). The mean error of the needle tip was 3.9±1.7 mm. There were no punctures of critical nontarget structures. The mean procedure length was 33±12 min.

CONCLUSION
1.5 T augmented reality-navigated interventional MRI can provide accurate imaging guidance for perineural injections of the thoracic, lumbar, and hypogastric sympathetic plexus.

The small paravertebral sympathetic ganglia are located anterolaterally along the entire length of the vertebral column extending from the upper neck to the ganglion impar at the sacrococcygeal junction, which is the terminal ganglion of the sympathetic nervous system in the pelvis (1). The paravertebral sympathetic ganglia connect preganglionic nerves from the spinal cord with postganglionic fibers of thoracic abdominal and pelvic organs. The paravertebral sympathetic chain has an important role in regulating blood flow, digestion, sweating, and pain. The ganglia may be categorized into thoracic, lumbar, and hypogastric regions, the latter of which is located at the level of the lumbosacral junction.

Visceral, ischemic, neuropathic, and vascular pain in the abdomen and lower limbs that is clinically suspected to be mediated through the sympathetic ganglia may be diagnosed with paravertebral anesthetic blocks and subsequently treated with targeted chemical or thermal neurolysis of the thoracic, lumbar, and hypogastric sympathetic ganglia (2–5).

Due to risk of nontarget needle localization, image-guidance is generally considered best practice for performing these thoracic or lumbar ganglion procedures. There is no consensus regarding the preferred modality for image guidance for sympathetic interventions. Authors have reported using fluoroscopy for thoracolumbar ganglion targeting (6–8). Few studies have assessed the use of computed tomography (CT) guidance and one study magnetic resonance imaging (MRI) guidance at 0.2 Tesla (T) low field strength (9–11). In contrast to the other imaging modalities, MRI-guided intervention provides the theoretical

This research was supported by the National Cancer Institute (grant 1 R01 CA118371-01A2).

From the Russel H. Morgan Department of Radiology and Radiological Science (D.R.M., J.A.C., J.F. ✉ *jfritz9@jhmi.edu*) and Mechanical Engineering and Laboratory for Computational Sensing and Robotics (I.I.I.), Johns Hopkins University School of Medicine, Baltimore, Maryland, USA; the Department of Mechanical and Materials Engineering (P.U.T.), and the School of Computing (T.U., G.F.), Queen's University, Kingston, Ontario, Canada; Siemens Corporate Research (A.J.F.), Center for Applied Medical Imaging, Baltimore, Maryland, USA.

Received 22 June 2016, revision requested 29 September 2016, last revision received 19 December 2016, accepted 3 January 2017.

Published online 18 April 2017.
DOI 10.5152/dir.2017.16323

advantages of highest soft tissue contrast, true multiplanar capabilities, and the use of nonionizing radiation exposure to the patient and interventional physician (12, 13).

However, open low-field MRI scanners may only provide limited spatial, temporal and contrast resolution, whereas closed-bore magnets with higher field strength offer better image quality, but have limited patient access (14, 15). Owing to the fact that magnetic resonance (MR) images can be acquired inside the closed-bore MRI scanner and projected onto the patient outside the bore, the potential barrier of patient access may be removed with the use of an augmented reality system (16, 17).

Therefore, we sought to assess the feasibility and initial technical performance of an augmented-reality MRI technique coupled with existing closed-bore MRI technology as a novel approach for perineural injections of the thoracic, lumbar, and hypogastric sympathetic ganglia.

Methods

Our study complied with the 1964 Helsinki declaration and its later amendments, Health Insurance Portability and Accountability Act, and state regulations for research with human cadavers. Internal review board approval was not required as no living subjects participated.

Twelve nonembalmed, full torso human cadavers (seven women, five men) were utilized. The median age at time of death was 75 years (range, 50–99 years). Based on living body mass index (BMI), there was an equal number of small (defined as living BMI of 16–18.5 kg/m^2), medium (18.5–25 kg/m^2) and large (25–30 kg/m^2) subjects with four cadavers in each size group. A total of 23 bilateral paravertebral sympathetic injections were planned at the thoracic (8/23, 35%), lumbar (8/23, 35%), and hypogastric (7/23, 30%) levels.

All procedures were performed with a 1.5 T MRI scanner (Magnetom Espree, Siemens Healthcare) (18) and flexible, receive only, surface loop coil of 19 cm diameter (Siemens Healthcare). The cadavers were placed prone in the table of the MRI scanner. MRI-compatible needle of 10 or 15 cm length and 20 Gauge thickness (MReye®, Cook Medical) were used with adjustable clip-on depth gauge for planned insertion depth. Punctures were performed by an interventional radiologist skilled in image-guided needle placement under augmented reality-assisted MRI navigation outside the bore of the MRI scanner (Fig. 1) (19).

High-resolution 3D turbo spin-echo MRI data sets (repetition time [TR], 1000-1100; echo time [TE], 34; flip angle [FA], 120; number of averages [Av], 2; echo train length [ETL], 73; slice thickness [ST], 1 mm; number of slices [SL], 240; field of view [FOV], 192×192 mm; base resolution [BR], 192 pixels; phase resolution [PR], 100%; and bandwidth [BW], 751 Hz) using a SPACE (Sampling Perfection with Application optimized Contrasts using different flip angle Evolution) pulse sequence were obtained of the thoracic, lumbar, and sacral spine for visualization of the paravertebral sympathetic plexus, definition of the puncture target point and planning of the most appropriate needle path. The isotropic 3D MR images were transferred into the navigation module (PerkStation) of the 3D Slicer software for interactive 3D evaluation of the anatomy using its DICOM viewer function. Using this navigation software, the operator marked the target point for final needle tip location next to the paravertebral sympathetic plexus and the desired skin entry point and the system plotted the needle path virtually. A dorsolateral paravertebral approach was used for all levels. Using the motorized table of the MRI scanner, the specimen was then moved out of the bore under the image-overlay navigation system so that the physical location of the target point inside the subject perfectly matched with the position of the navigation system, which was indicated by a laser line that was projected on the specimen. The MR image containing the target and the virtual needle path was then projected through the image-overlay navigation system onto a semitransparent mirror. By looking at the subject through the semitransparent mirror of the image-overlay navigation system, a matching hybrid or augmented reality im-

Main points

- Augmented reality image-overlay navigation provides the operator with a hybrid view of the patient and co-registered image, which contains the target and needle path information for needle placement.
- Augmented reality image-overlay navigation facilitates out-of-bore guidance for interventional MRI procedures.
- Augmented reality-navigated interventional MRI can provide accurate imaging guidance for perineural injections of the thoracic, lumbar, and hypogastric sympathetic plexus.

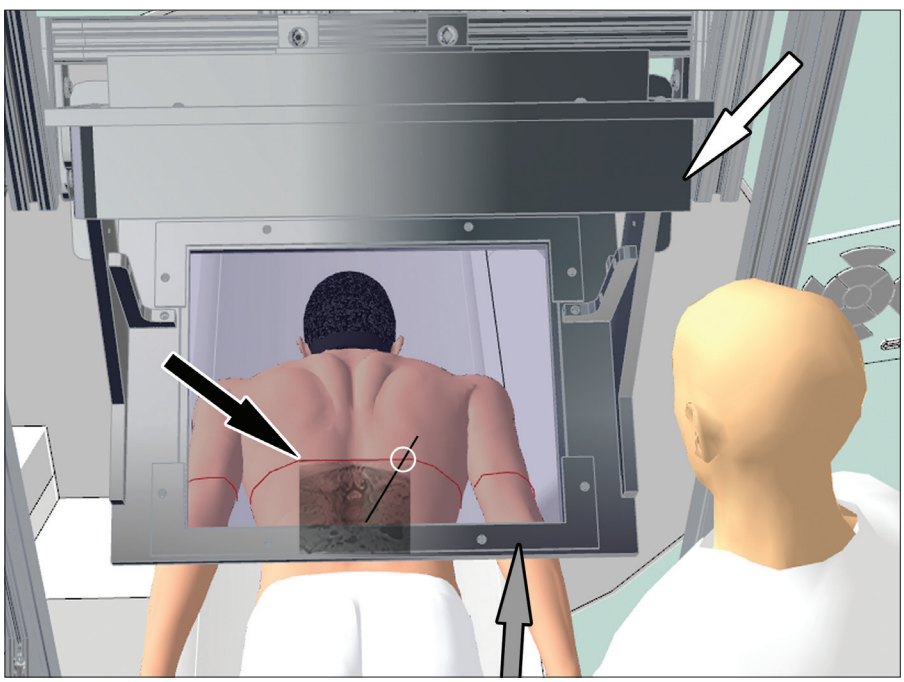

Figure 1. Three-dimensional illustration in bird's-eye-view showing the operator and augmented reality navigation system with display *(white arrow)* and semi-transparent mirror, which reflects the projected magnetic resonance (MR) image containing the needle path into the line of sight of the operator creating a hybrid image of MR image and subject. The red laser line *(black arrow)* on the subject's skin marks the target image plane in the craniocaudal direction and provides the second dimension of the skin entry point.

age was being created of cadaver and MR image (Fig. 2). The image-overlay navigation system matched the exact location, size and skin contour between MR image and cadaver specimen. The previously selected skin entry point was automatically displayed to the operator as the intersection of the laser that was projected on to the specimen's skin and the displayed virtual needle path and subsequently targeted by looking through the semi-transparent mirror. No manual measurements were needed. Outside of the bore and under the image-overlay navigation system, the needle was inserted along the virtual trajectory to the target. Using the motorized table of the MRI scanner, the cadavers were intermittently moved back inside the bore to assess and document needle tip positions using a turbo spin-echo pulse sequence (TR, 1200; TE, 12; FA, 120; Av, 1; ETL, 17; ST, 3 mm; SL, 5; FOV, 256×224 mm; BR, 320 pixels; PR, 100%; BW, 252 Hz). Following satisfactory needle placement, a total of 5 mL of gadolinium-containing saline solution (1:250) was injected at each site, which was monitored with real-time MRI fluoroscopy using a gradient echo pulse sequence (TR, 9.3; TE, 3.5; FA, 60; Av, 1; ST, 5 mm; FOV, 256×224 mm; BR, 256; PR, 56%; BW, 180 Hz). After the injections were completed, T1-weighted, fat-suppressed MR images (TR, 500; TE, 12; FA, 120; Av, 1; ETL, 17; ST, 3 mm; SL, 7; FOV, 256×224 mm; BR, 320 pixels; PR, 100%; BW, 252 Hz) were obtained to confirm the location of the injected gadolinium-enhanced solution.

Technical performance parameters were assessed for each needle placement individually and included the number of control MR images and adjustments that were needed for advancing the needle to the target location, the target error of the final needle tip location, puncture of critical nontargeted structures such as the pleura, aorta, common and external iliac arteries, and the rate of successful delivery of the injectant. The length of time was assessed for each level and included the time needed for bilateral injections at the respective level, including planning of the needle path bilaterally, as well as completing needle placement and injection bilaterally. The needle adjustment rate was further stratified by assessing removal and new placement (reinsertion), adjustment of needle trajectory (trajectory change), and needle withdrawal for depth (withdrawal) in a straight fashion. The error of the needle tip relative to the target was measured as the distance of the needle tip between the virtual and final position, which was measured automatically during the session by the PerkStation navigation module after the operator manually defined the needle tip. Intermittently obtained MR images were evaluated for inadvertent puncture of vulnerable structures and for the thoracic region, postprocedural images were assessed for the occurrence of a pneumothorax. If a pneumothorax was present in the beginning, leakage of contrast into the thoracic cavity was used

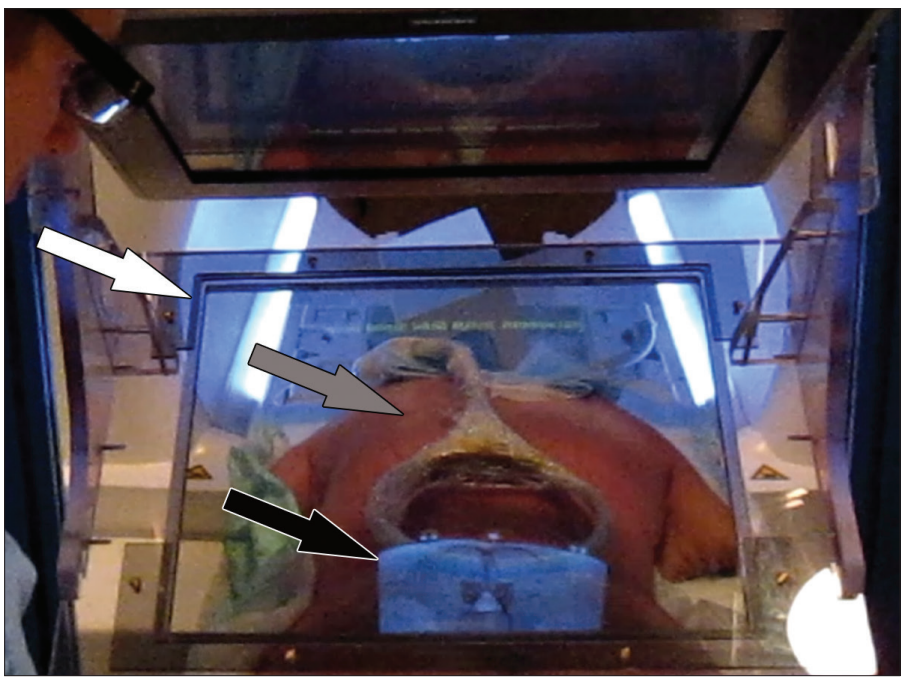

Figure 2. Procedural photograph demonstrating the operator's augmented reality consisting of a hybrid view of MR image and underlying cadaver. The hybrid view is being created by the reflection of the target MR image *(black arrow)* from a semitransparent mirror *(white arrow)* into the line of sight of the operator, where it merges with the underlying cadaver *(gray arrow)*. Location, size, and skin contour of MR image and cadaver are matched through co-registration by the image-overlay navigation system.

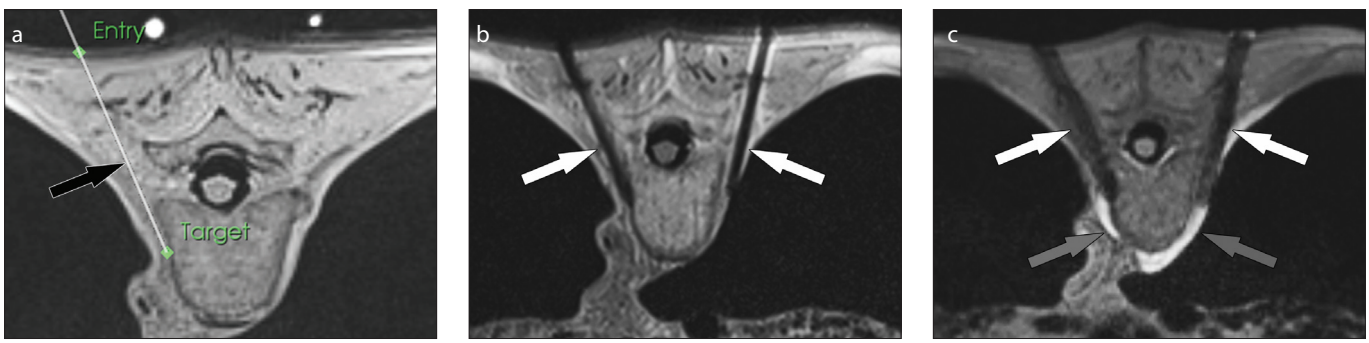

Figure 3. a–c. MRI-guided thoracic paravertebral sympathetic plexus injection. Axial intermediate-weighted MR image **(a)** demonstrates the virtual needle path *(arrow)* to the right paravertebral sympathetic plexus connecting the virtual skin entry and target points. Axial intermediate-weighted turbo spin-echo MR image **(b)** demonstrates the tips of the needles *(arrows)* in the paravertebral space where the sympathetic nerve plexus resides. Axial gradient echo image frame **(c)** of real-time MRI monitoring of the injection shows the needles *(white arrows)* and the hyperintense injectant *(gray arrows)* accumulating in paravertebral space and around the sympathetic nerve plexus.

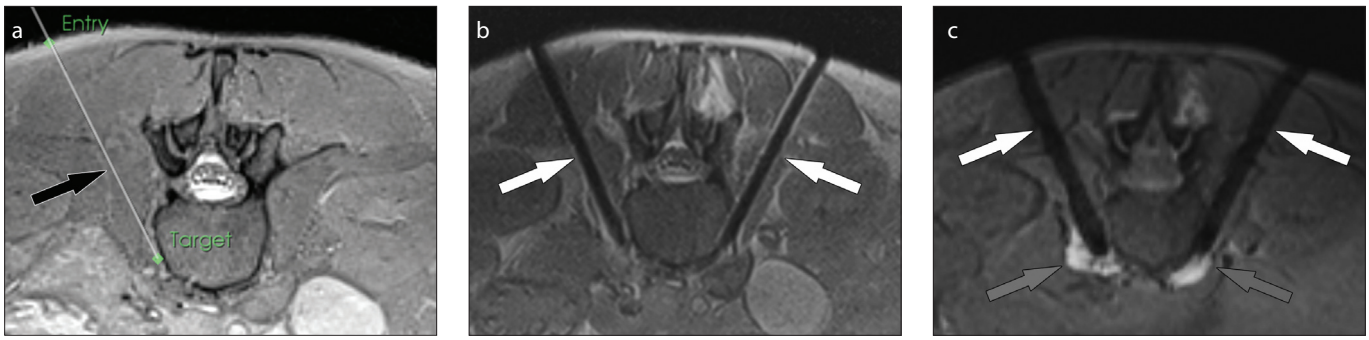

Figure 4. a–c. MRI-guided lumbar paravertebral sympathetic plexus injection. Axial intermediate-weighted MR image **(a)** demonstrates the virtual needle path *(arrow)* to the right paravertebral sympathetic plexus connecting the virtual skin entry and target points. Axial intermediate-weighted turbo spin-echo MR image **(b)** demonstrates the tips of the needles *(arrows)* in the paravertebral space where the sympathetic nerve plexus resides. Axial gradient echo image frame **(c)** of real-time MRI monitoring of the injection shows the needles *(white arrows)* and the hyperintense injectant *(gray arrows)* accumulating in paravertebral space and around the sympathetic nerve plexus.

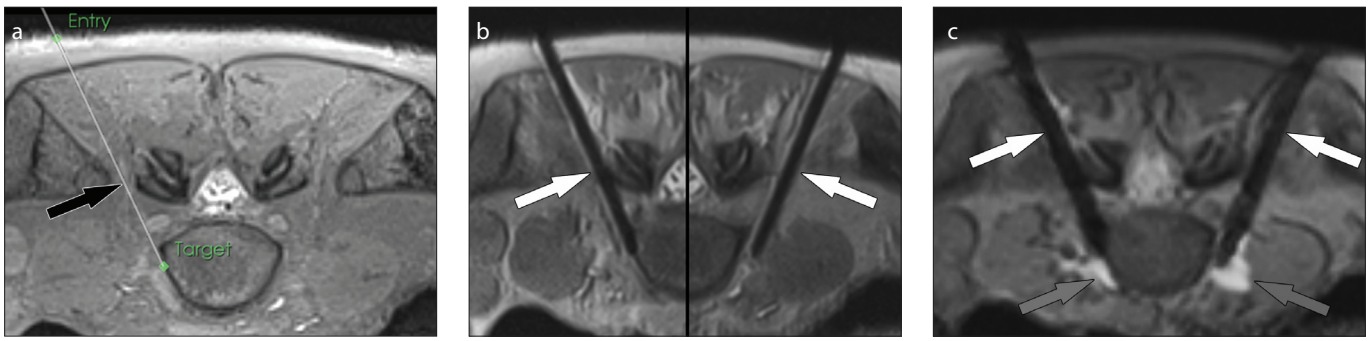

Figure 5. a–c. MRI-guided hypogastric paravertebral sympathetic plexus injection. Axial intermediate-weighted MR image **(a)** demonstrates the virtual needle path *(arrow)* to the right paravertebral sympathetic plexus at the lumbosacral junction connecting the virtual skin entry and target points. Axial intermediate-weighted turbo spin-echo MR image **(b)** demonstrates the tips of the needles *(arrows)* in the paravertebral space where the sympathetic nerve plexus resides. Axial gradient echo image frame **(c)** of real-time MRI monitoring of the injection shows the needles *(white arrows)* and the hyperintense injectant *(gray arrows)* accumulating in paravertebral space and around the sympathetic nerve plexus.

as a surrogate marker for injury of the pleural cavity.

The collected data were entered into a spreadsheet format. Standard Excel (Microsoft Inc.) functionality was utilized for aggregating the data. The spreadsheet data was imported into IBM SPSS Statistics for Windows, version 22 (IBM Corp.) for additional data analysis and statistical calculations. The Kolmogorov-Smirnov test was used for the normality test including Lilliefors significance correction. Variables were expressed as frequencies and proportions as well as mean and first standard deviation for data with normal distribution or median with minimum and maximum for data without normal distribution. Results were stratified by target location (paravertebral thoracic sympathetic plexus, paravertebral lumbar sympathetic plexus, and lumbosacral hypogastric plexus) as well as by the three groups of cadaver size based on BMI. The Fisher-Freeman-Halton test was utilized to assess for any differences in the outcomes for these subgroups. *P* values of less than 0.05 were considered statistically significant.

Results

All planned punctures (46/46, 100%) were carried out successfully in all three cadaver sizes and at all spinal levels (Figs. 3–5). Turbo spin-echo MR images successfully provided documentation of needle tip positions. An average of two (range, 1–5) intermittent MRI control steps was required to place a needle. There were nine trajectory adjustments of the needle (20%) and six advancements (13%). There were no reinsertions. The average distance of the needle tip to the virtual target was 3.9±1.7 mm [coefficient of variance, 10.2±4.5%; range, 1.6%–20.9%]. No punctures of nontarget structures occurred. Specifically, there was no evidence for injury of the pleural cavity. Gradient echo real-time MRI demonstrated successful injectant delivery and perineural spread for all targets (46/46, 100%). The mean procedure time for one level including bilateral injections was 33±12 min. The number of control MR images needed for needle placement, needle adjustment rates, error of the tip to target, rate of puncture of nontarget structures, successful injectant delivery rate, and procedure length were similar across all groups (Table).

Discussion

We have demonstrated the feasibility and initial technical performance of 1.5 T MRI-guided paravertebral sympathetic injections in human cadavers utilizing augmented reality navigation. Turbo spin-echo sequences that were optimized for metal artifact reduction resulted in an accurate display of the needle location and needle placements into the paravertebral space with a target error about 4 mm. MRI fluoroscopy monitoring was successfully used to demonstrate the distribution of the injected fluid and accumulation in the paravertebral space in which the sympathetic ganglia reside. There were no punctures of critical nontarget structures.

The underlying premise for using imaging guidance is accurate needle placement in order to provide optimal treatment while avoiding complications. Historically, paravertebral sympathetic blocks were performed using anatomic landmarks as guidance but there was no reliable technique to determine the needle end-point. Results of these

Table. Comparison of technical parameters stratified by spinal level and body mass subgroups

Subgroups	Needle adjustment type		*P*
	Trajectory change		
Spinal levels	Yes	No	
Thoracic	4	12	0.728
Lumbar	2	14	
Lumbosacral	3	11	
	Advancement		
Spinal levels	Yes	No	
Thoracic	2	14	0.860
Lumbar	3	13	
Lumbosacral	1	13	
	Trajectory change		
Body mass subgroup	Yes	No	
Small	4	12	0.893
Medium	3	13	
Large	2	12	
	Advancement		
Body mass subgroup	Yes	No	
Small	2	14	0.859
Medium	1	15	
Large	3	13	

blind techniques are suboptimal. In cadaveric models, the blind techniques has sometimes resulted in pleural and renal needle localization (20); however, image guidance does not completely eliminate the risks associated with paravertebral sympathetic blocks. Studies have reported several complications, such as genitofemoral neuralgia, necrosis of the psoas muscle, injury of the kidney and ureter, bleeding, hypotension and impotence, permanent lesion to the lateral femoral cutaneous nerve, hemopneumothorax, priapism, Horner's syndrome, and massive retroperitoneal hematoma (21–26).

In addition, there are unique risks both to the patient and the operator associated with modalities that utilize ionizing radiation (27), and consideration for MRI-guided procedures may have particular relevance for patients who are younger or may require repeat procedures (28). The present study showed that the combination of image-overlay navigation and the image quality of interventional MRI at 1.5 T was able to readily define accurate needle paths and provide safe needle guidance in all cases. A patient study is required to ascertain whether these findings translate to a low complication rate in patients.

Currently there are limited clinical studies regarding the efficacy of MRI-guided sympathetic interventional therapy (10, 29, 30). König et al. (10) assessed clinical outcomes of low-field MRI-guided paravertebral lumbar sympathetic neurolysis. The authors performed 101 MRI-guided procedures in 89 patients using a dedicated, horizontally open 0.2 T MRI scanner. There was a 90% success rate with 10 patients not treated due to patient discomfort (n=4), motion degradation of images (n=4), osteophytosis of the spine (n=1), and retroperitoneal hemorrhage (n=1). One case of ureteral necrosis occurred. A total of 3.5 pulse sequences were acquired for needle placement. Table time was 32.3 min. In addition to paravertebral sympathetic targeting, the celiac plexus is often targeted to treat visceral pain related to cancer. Hol et al. (29) reported using a 0.5 T open MRI scanner with "double-donut" design and optical tracking system to perform celiac plexus blocks for palliation of patients with severe upper abdominal pain due to pancreatitis or tumors of the pancreas. They reported good or complete pain relief in eight of 14 blocks (57%), a moderate effect in five blocks (36%), and no effect in one block (7%). Aside from the limited availability of the above used open MRI scanners, because they are no longer commercially available, primary differences to the closed bore 1.5 T MRI scanner used in the present study are related to the lower field strength, which results in less homogeneity, lower MRI signal, limited image quality and longer imaging times. The augmented reality system used in the present study was able to overcome the barrier of patient access inherent to the closed bore magnet design, which may also be used with modern 3.0 T MRI scanners (31, 32).

The limitations of this study include the lack of patient motion and respiration. However, given the paravertebral location of the targets, with use of light sedation, respiratory and patient motion would likely be minor factors. The procedure time in the study did not exactly reflect the clinical practice in that it did not include time for setting up and taking down the navigation system if the magnet was also going to be used for diagnostic imaging. This, however, could be addressed by use of block time where several patients are treated consecutively or by use of a self-calibrating mobile navigation system, which essentially requires no additional set-up time (33). Despite these limitations, the results of this study are promising and suggest that augmented reality navigated 1.5 T MRI guided paravertebral injections are technically feasible at multiple spinal levels and can provide accurate needle placement for paravertebral sympathetic ganglion targeting.

In conclusion, MRI-guided paravertebral approach for thoracic, lumbar, and hypogastric sympathetic plexus targeting is feasible at 1.5 T and provides accurate and consistent image guidance. Interventional MRI at 1.5 T field strength allows visualization of soft tissue anatomy, which facilitates avoidance of nontarget injection. Injectants are well visualized, which allows the interventionalist to readily confirm successful anatomic localization of the block. *In vivo* studies are needed to confirm the safety and efficacy of this technique.

Conflict of interest disclosure

The authors declared no conflicts of interest. Jan Fritz received institutional research funds and speaker's honorarium from Siemens Healthcare USA and is a scientific advisor of Siemens Healthcare USA and Alexion Pharmaceuticals, Inc., outside the submitted work. John a Carrino is a consultant to Pfizer, Globus Medical, ADX and an advisor to General Electric, Carestream, Halyard Health, outside the submitted work.

References

1. Marker DR, U-Thainual P, Ungi T, et al. MR-guided perineural injection of the ganglion impar: technical considerations and feasibility. Skeletal Radiol 2016; 45:591–597. [CrossRef]
2. Kosugi S, Hashiguchi S, Nishimura D, et al. Neurolysis targeting both the aorticorenal ganglia and lumbar sympathetic plexus for kidney tumor-related pain. Pain Med 2015; 16:202–203. [CrossRef]
3. Rocha Rde O, Teixeira MJ, Yeng LT, et al. Thoracic sympathetic block for the treatment of complex regional pain syndrome type I: A double-blind randomized controlled study. Pain 2014; 155:2274–2281. [CrossRef]
4. Dominkus M, Kepplinger B, Bauer W, Dubsky E. Percutaneous radiofrequency thermolesion of the sympathetic chain in the treatment of peripheral vascular disease. Acta Med Austriaca 1991; 18 Suppl 1:69–70.
5. Straube S, Derry S, Moore RA, Cole P. Cervico-thoracic or lumbar sympathectomy for neuropathic pain and complex regional pain syndrome. Cochrane Database Syst Rev 2013; 9:CD002918. [CrossRef]
6. Yoo HS, Nahm FS, Lee PB, Lee CJ. Early thoracic sympathetic block improves the treatment effect for upper extremity neuropathic pain. Anesth Analg 2011; 113:605–609. [CrossRef]
7. Hong JH, Kim AR, Lee MY, Kim YC, Oh MJ. A prospective evaluation of psoas muscle and intravascular injection in lumbar sympathetic ganglion block. Anesth Analg 2010; 111:802–807. [CrossRef]
8. Sprague RS, Ramamurthy S. Identification of the anterior psoas sheath as a landmark for lumbar sympathetic block. Reg Anesth 1990; 15:253–255.
9. Schmid MR, Kissling RO, Curt A, Jaschko G, Hodler J. Sympathetic skin response: monitoring of CT-guided lumbar sympathetic blocks. Radiology 2006; 241:595–602. [CrossRef]
10. Konig CW, Schott UG, Pereira PL, et al. MR-guided lumbar sympathicolysis. Eur Radiol 2002; 12:1388–1393. [CrossRef]
11. Wilsey C, Ashford NS, Dolin SJ. Presacral neurolytic block for relief of pain from pelvic cancer: description and use of a CT-guided lateral approach. Palliat Med 2002; 16:441–444. [CrossRef]
12. Braun J, Bollow M, Seyrekbasan F, et al. Computed tomography guided corticosteroid injection of the sacroiliac joint in patients with spondyloarthropathy with sacroiliitis: clinical outcome and followup by dynamic magnetic resonance imaging. J Rheumatol 1996; 23:659–664.
13. Konig CW, Trubenbach J, Fritz J, Lauer UM, Claussen CD, Pereira PL. Contrast enhanced MR-guided biopsy of hepatocellular carcinoma. Abdom Imaging 2004; 29:71–76. [CrossRef]
14. Fritz J, Tzaribachev N, Thomas C, et al. Magnetic resonance imaging-guided osseous biopsy in children with chronic recurrent multifocal osteomyelitis. Cardiovasc Intervent Radiol 2012; 35:146–153. [CrossRef]
15. Konig CW, Trubenbach J, Bohm P, Fritz J, Duda SH, Pereira PL. Magnetic resonance-guided transcortical biopsy of bone marrow lesions using a magnetic resonance imaging-compatible piezoelectric power drill: preliminary experience. Invest Radiol 2003; 38:159–163. [CrossRef]
16. Wacker FK, Vogt S, Khamene A, et al. An augmented reality system for MR image-guided needle biopsy: initial results in a swine model. Radiology 2006; 238:497–504. [CrossRef]
17. Sequeiros RB, Klemola R, Ojala R, Jyrkinen L, Vaara T, Tervonen O. Percutaneous MR-guided discography in a low-field system using optical instrument tracking: a feasibility study. J Magn Reson Imaging 2003; 17:214–219. [CrossRef]
18. Weiss CR, Marker DR, Fischer GS, Fichtinger G, Machado AJ, Carrino JA. Augmented reality visualization using Image-Overlay for MR-guided interventions: system description, feasibility, and initial evaluation in a spine phantom. AJR Am J Roentgenol 196:W305–307. [CrossRef]
19. Fritz J, U-Thainual P, Ungi T, et al. Augmented reality visualization with image overlay for MRI-guided intervention: accuracy for lumbar spinal procedures with a 1.5-T MRI system. AJR Am J Roentgenol 2012; 198:W266–273. [CrossRef]
20. Cherry DA, Rao DM. Lumbar sympathetic and coeliac plexus blocks. An anatomical study in cadavers. Br J Anaesth 1982; 54:1037–1039. [CrossRef]
21. Sniderman M, Raghavendra M, Holtman JR, Jr. Priapism following a lumbar sympathetic nerve block. Pain Med 12:1046–1048. [CrossRef]
22. Maranhao-Filho PA, Martins MA, Lopes HF. Horner's syndrome and brachial paresis as a complication of lumbar sympathetic block: a case report. Arq Neuropsiquiatr 1995; 53:831–833. [CrossRef]
23. Pennekamp W, Krumova EK, Feigl GP, et al. Permanent lesion of the lateral femoral cutaneous nerve after low-volume ethanol 96% application on the lumbar sympathetic chain. Pain Physician 2013; 16:391–397.
24. Sakai T, Sano A, Matsukura A, et al. Hemopneumothorax after thoracic sympathetic nerve block; report of a case. 2014; Kyobu Geka 67:599–601.
25. Maier C, Gleim M, Weiss T, Stachetzki U, Nicolas V, Zenz M. Severe bleeding following lumbar sympathetic blockade in two patients under medication with irreversible platelet aggregation inhibitors. Anesthesiology 2002; 97:740–743. [CrossRef]
26. Hong JH, Oh MJ. Comparison of multilevel with single level injection during lumbar sympathetic ganglion block: efficacy of sympatholysis and incidence of psoas muscle injection. Korean J Pain 2010; 23:131–136. [CrossRef]
27. Wagner LK. CT fluoroscopy: another advancement with additional challenges in radiation management. Radiology 2000; 216:9–10. [CrossRef]
28. Fritz J, U-Thainual P, Ungi T, et al. Augmented reality visualization with use of image overlay technology for MR imaging-guided interventions: assessment of performance in cadaveric shoulder and hip arthrography at 1.5 T. Radiology 2012; 265:254–259. [CrossRef]
29. Hol PK, Kvarstein G, Viken O, Smedby O, Tonnessen TI. MRI-guided celiac plexus block. J Magn Reson Imaging 2000; 12:562–564.
30. Sze DY, Mackey SC. MR guidance of sympathetic nerve blockade: measurement of vasomotor response initial experience in seven patients. Radiology 2002; 223:574–580. [CrossRef]
31. Fritz J, Dellon AL, Williams EH, Belzberg AJ, Carrino JA. 3-Tesla high-field magnetic resonance neurography for guiding nerve blocks and its role in pain management. Mag Reson Imaging Clin N Am 2015; 23:533–545. [CrossRef]
32. Fritz J, Chhabra A, Wang KC, Carrino JA. Magnetic resonance neurography-guided nerve blocks for the diagnosis and treatment of chronic pelvic pain syndrome. Neuroimaging Clin N Am 2014; 24:211–234. [CrossRef]
33. Anand M, King F, Ungi T, et al. Design and development of a mobile image overlay system for needle interventions. Conf Proc IEEE Eng Med Biol Soc 2014; 2014:6159–6162. [CrossRef]